Photoelectrochemistry

Deutsche Ausgabe: DOI: 10.1002/ange.201700117
Internationale Ausgabe: DOI: 10.1002/anie.201700117

Highly Active GaN-Stabilized Ta_3N_5 Thin-Film Photoanode for Solar Water Oxidation

*Miao Zhong, Takashi Hisatomi, Yutaka Sasaki, Sayaka Suzuki, Katsuya Teshima, Mamiko Nakabayashi, Naoya Shibata, Hiroshi Nishiyama, Masao Katayama, Taro Yamada, and Kazunari Domen**

Abstract: *Ta_3N_5 is a very promising photocatalyst for solar water splitting because of its wide spectrum solar energy utilization up to 600 nm and suitable energy band position straddling the water splitting redox reactions. However, its development has long been impeded by poor compatibility with electrolytes. Herein, we demonstrate a simple sputtering-nitridation process to fabricate high-performance Ta_3N_5 film photoanodes owing to successful synthesis of the vital TaO_δ precursors. An effective GaN coating strategy is developed to remarkably stabilize Ta_3N_5 by forming a crystalline nitride-on-nitride structure with an improved nitride/electrolyte interface. A stable, high photocurrent density of 8 mA cm^{-2} was obtained with a CoPi/GaN/Ta_3N_5 photoanode at 1.2 V_{RHE} under simulated sunlight, with O_2 and H_2 generated at a Faraday efficiency of unity over 12 h. Our vapor-phase deposition method can be used to fabricate high-performance (oxy)nitrides for practical photoelectrochemical applications.*

Solar energy is a clean and abundant source of energy available over the entire planet. The efficient storage of intermittent solar energy as renewable hydrogen fuels by photoelectrochemical (PEC) water splitting represents a potentially sustainable means of meeting worldwide energy demands with limited environmental pollution.[1–6] However, challenges related to the development of high-performance photoanodes have long thwarted the practical applications of water splitting devices.[7,8]

Photoanodic materials intended for water splitting should possess several important properties, including suitable energy band positions, absorption of long wavelength light, efficient charge separation and high catalytic activity. Because they offer wider absorption spectra than metal oxides and more favorable energy band positions for water splitting than group IV, III–V, and II–VI solar cell materials, metal (oxy)-nitrides, such as TaON,[9] Ta_3N_5,[10] $LaTiO_2N$,[11] $BaTaO_2N$,[12] and $SrNbO_2N$,[13] have been intensively studied as photoanodes. However, the lifespans of these (oxy)nitrides during operation in an actual electrolyte remain poor. Therefore, this lack of stability over long-term use is a critical issue that must be addressed before the industrialization of these materials.

(Oxy)nitride photoanodes are operated in highly oxidizing environments that thermodynamically favor photocorrosion to form resistive surface oxides. Once they grow to depths of several tens of nanometers, these defective oxide layers can lead to significant charge recombination and act as insulators to reduce the charge transfer across the photoanode/electrolyte interface. The removal of surface oxides by washing (oxy)nitrides in acidic solutions greatly improves PEC performance,[14–16] although this improved performance rapidly drops off again as the materials once more undergo the self-oxidation that readily occurs in harsh oxidizing environments during water oxidation. For this reason, applying a thin protective layer that prevents direct contact of the (oxy)nitride with the electrolyte while effectively transferring the charges for water oxidation is crucial. One successful approach has been to deposit oxygen evolution reaction (OER) co-catalysts, such as NiOOH,[17] FeOOH,[18] and CoPi[19] to extract photogenerated holes in the (oxy)nitrides, thus alleviating photocorrosion. However, due to the ion-permeable nature of OER co-catalysts, it is difficult to permanently isolate (oxy)nitrides from hydroxy ions in water to ensure long-term stability. We propose to overcoat (oxy)nitrides with a thin nitride film to generate an inherently nitrogen-rich and buried nitride/nitride interface that will prevent photocorrosion. The resulting well-passivated nitride/electrolyte interface can further improve both the onset potential and photocurrent density for solar water splitting.

Among the nitrides that could be applied in this manner, GaN is particularly interesting. First, GaN is relatively stable against corrosion[20–22] compared to other nitrides. Over 100 h of PEC water splitting has been achieved with NiO coated GaN photoanodes in alkaline media.[22] Second, the conduction band of GaN is more negative than those of Ta_3N_5, $BaTaO_2N$, $LaTiO_2N$ and $SrNbO_2N$, which tends to mitigate the migration of photogenerated electrons to the GaN on a thermodynamic basis, thus reducing charge recombination.[21,23,24] Third, GaN has a long hole lifetime of 10–500 ns[25–28] that is superior to the lifetimes of (oxy)nitrides, which are generally below 10 ns.[29,30] Reduced charge recombination and improved hole mobility in GaN are critical

[*] Dr. M. Zhong, Prof. T. Hisatomi, Y. Sasaki, M. Nakabayashi, Prof. N. Shibata, Prof. H. Nishiyama, Prof. M. Katayama, Prof. T. Yamada, Prof. K. Domen
School of Engineering, the University of Tokyo
7-3-1 Hongo, Bunkyo-ku, Tokyo 113-8656 (Japan)
and
Japan Technological Research Association of Artificial Photosynthetic Chemical Process
2-11-9 Iwamotocho, Chiyoda-ku, Tokyo 101-0032 (Japan)
E-mail: domen@chemsys.t.u-tokyo.ac.jp
Dr. S. Suzuki, Prof. K. Teshima
Faculty of Engineering, Shinshu University
4-17-1 Wakasato, Nagano 380-8553 (Japan)
Supporting information and the ORCID identification number(s) for the author(s) of this article can be found under: http://dx.doi.org/10.1002/anie.201700117.

semiconducting properties that allow the development of efficient (oxy)nitride photoanodes. Last, we affirmed that crystalline GaN-on-Ta_3N_5 structures can be synthesized via high-temperature processes, without forming defective bimetallic phases, to improve the PEC stability and performances.

In the present study, we developed an effective sputtering-nitridation process for synthesis of high-performance Ta_3N_5 thin film photoanodes capable of generating a photocurrent density of 7.5 mA cm^{-2} at 1.2 V vs. a reversible hydrogen electrode (V_{RHE}) under simulated sunlight illumination in conjunction with CoPi co-catalysts. However, a highly resistive TaO_x layer was formed on Ta_3N_5 surfaces during PEC water oxidation, degrading the PEC performance of CoPi/Ta_3N_5 within a span of 1 h. We demonstrated that coating the Ta_3N_5 film with a 50 nm thick crystalline GaN layer can significantly stabilize its solar water splitting performance. A stable, high photocurrent density of 8 mA cm^{-2} was obtained with a CoPi/GaN/Ta_3N_5 photoanode at 1.2 V_{RHE} under solar light illumination over 10 h. The onset potential of the CoPi/GaN/Ta_3N_5 was further cathodically improved by 150 mV owing to passivation of the Ta_3N_5 surface states as evidenced by Mott–Schottky analyses with a proposed band bending diagram. The results herein represent one of the highest stable solar water splitting performances obtained from a Ta_3N_5 thin film photoanode (see the comparison in Table S1), with stoichiometric O_2 and H_2 generated at a Faraday efficiency of unity over 12 h. Long-term PEC stability can be anticipated by coating conformal GaN on Ta_3N_5 and also on other promising (oxy)nitrides. Our nitride-on-nitride structure incorporating crystalline interfaces offers a new paradigm for future development of various efficient and stable (oxy)nitride photoanodes for practical applications.

Nanocrystalline Ta_3N_5 films were fabricated on Ta substrates by a simple sputtering and nitridation process, as shown in detail in the Experimental Section and Figure S1 in the Supporting Information. In the initial step, an about 500 nm thick TaO_δ precursor film (containing a limited amount of O) was sputtered on a Ta substrate. Precise control of the O amount incorporated during sputtering of the TaO_δ is important for ensuring the subsequent synthesis of high-performance Ta_3N_5. The sputtered TaO_δ precursors were identified by XRD patterns, sheet resistivity in Table 1 and XPS spectra in Figure S2. Details of each TaO_δ are discussed in the supporting information. Starting from the TaO_δ-b precursor, the synthesized Ta_3N_5 has a monoclinic crystal structure without any formation of σ-TaN, Ta_2N or Ta_5N_6 (all representing tetragonal crystal structures), or other tantalum nitrides[31] (Figure S3). A high photocurrent density of 7–8 mA cm^{-2} was generated by this Ta_3N_5 at 1.2 V_{RHE} under simulated sunlight illumination with CoPi co-catalysts. The TaO_δ-a precursor was too metallic to synthesize pure Ta_3N_5 (Figure S3), and no PEC response was obtained with the resulting film (Figure S4). Monoclinic Ta_3N_5 was synthesized from the TaO_δ-c precursor but undesirable tetragonal TaN and Ta_5N_6 crystallites were also formed (Figure S3). The PEC performance was also reduced to 4 mA cm^{-2} at 1.2 V_{RHE} (Figure S4). Further increase in the sheet resistivity of the sputtered precursor significantly decreased the photocurrent density to 1 mA cm^{-2} after nitridation of the highly resistive sputtered TaO_x under the same nitridation conditions (Figure S5b).

The chemical states of Ta and O in the sputtered TaO_δ-a, TaO_δ-b, TaO_δ-c and TaO_x (sheet resistivity $>10^6\ \Omega$) were examined by XPS analyses. For comparison, the XPS spectra of Ta metal and Ta_2O_5 powder were also recorded. As shown in Figure S2d, binding energy peaks at 21.5 and 23.3 eV attributed to Ta $4f_{7/2}$ and Ta $4f_{5/2}$ in metallic Ta and at 26.4 and 28.2 eV attributed to Ta $4f_{7/2}$ and Ta $4f_{5/2}$ in Ta_2O_5 or TaO_x were observed. Binding energy peaks of O 1s at 530.8 eV were observed for all the sputtered films (Figure S2e). It is thus suggested that the sputtered precursors are composed of metallic Ta and amorphous TaO_x. Metallic Ta in TaO_δ films is observed in XRD patterns and amorphous TaO_x is evidenced by sheet resistivity measurements.

Cross-sectional TEM images of the highest performing Ta_3N_5 are shown in Figure 1, in which fine nanocrystalline Ta_3N_5 is clearly observed throughout the film. Moreover, the compact Ta_3N_5 film is closely attached to the conductive Ta substrate, enabling efficient electrical conductivity. As a result, high PEC performance was obtained. To stabilize the PEC output, GaN was coated onto the Ta_3N_5. As shown in Figure S1, uniform, 50 nm thick GaO_x coatings were applied to the Ta_3N_5/Ta films by electron beam (EB) evaporation. The GaO_x/Ta_3N_5/Ta samples were then nitrided in NH_3 at 1273 K for 0.5 h. As shown in the XRD patterns in Figure S6, GaN

Table 1: Sheet resistivity and main XRD peaks of TaO_δ precursors. Main XRD peaks and PEC performances of nitrided TaO_δ precursors with CoPi modifications. The sputtering conditions used with TaO_δ precursors are provided in the Experimental Section in the Supporting Information.

	Precursor TaO_δ-a	Precursor TaO_δ-b	Precursor TaO_δ-c
sheet resistivity	$10^0\ \Omega$	$10^1\ \Omega$	$10^2\ \Omega$
XRD of precursors	strong α-Ta, β-Ta peaks	broad α-Ta peak	broad α-Ta, β-Ta peaks
XRD after nitridation	strong β-Ta peaks	single-phase Ta_3N_5	Ta_3N_5 with TaN, Ta_5N_6
PEC performances	no PEC response	7–8 mA cm^{-2} at 1.2 V_{RHE}	4 mA cm^{-2} at 1.2 V_{RHE}

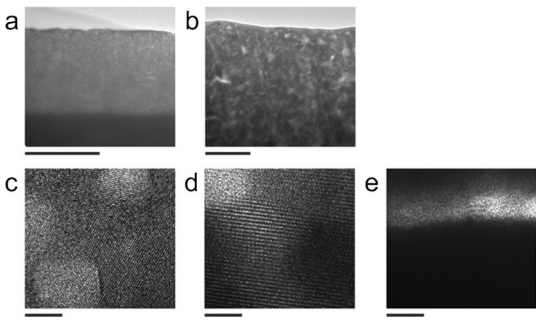

Figure 1. Cross-sectional TEM images of a Ta_3N_5 film on a Ta substrate synthesized by sputtering and nitridation. a) A Ta_3N_5 film on a Ta substrate, in which the scale bar is 500 nm, b) an enlarged magnification TEM image of the Ta_3N_5 film, in which the scale bar is 100 nm, and high magnification images of the c) surface, d) bulk, and e) bottom of a Ta_3N_5 film. The scale bars are 5 nm.

crystallites were formed on the Ta_3N_5 over a large scale without degrading the Ta_3N_5 crystallinity and any formation of defective bimetallic phases.

The PEC performance of the CoPi/GaN/Ta_3N_5 (with a 50 nm GaN layer) and CoPi/Ta_3N_5 photoanodes was investigated. The appearance of an anodic photocurrent was determined by reverse linear sweep voltammetry (LSV) scans from positive to negative potentials. The LSV scans in Figure 2a show that the onset potential for the CoPi/Ta_3N_5

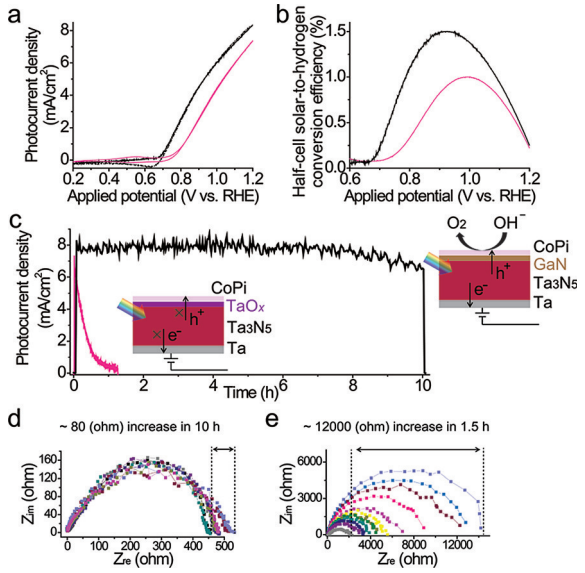

Figure 2. a) Linear sweep voltammetry (LSV) forward and backward scans of CoPi/GaN/Ta_3N_5 (black) and CoPi/Ta_3N_5 (pink) photoanodes in 0.5 M KPi solution at pH 13 under simulated solar light (AM 1.5G) illumination at a scan rate of 10 $mV s^{-1}$, b) hypothetical half-cell solar-to-hydrogen energy conversion efficiency of the CoPi/GaN/Ta_3N_5 (black) and CoPi/Ta_3N_5 (pink) photoanodes calculated from the LSV curves, c) time-course photocurrent density (*j*–*t*) curves for the CoPi/GaN/Ta_3N_5 (black) and CoPi/Ta_3N_5 (pink) photoanodes in 0.5 M KPi solutions at pH 13 under simulated solar light (AM 1.5G) illumination at 1.2 V_{RHE}, and Nyquist plots obtained at 1.2 V_{RHE} under AM 1.5G illumination in 0.5 M KPi at pH 13 for the d) CoPi/GaN/Ta_3N_5 and e) CoPi/Ta_3N_5 photoanodes. The color change from gray to pale purple indicates d) 1.5 h time intervals and e) 15 minutes time intervals.

photoanode was 0.8 V_{RHE}, which is similar to the previously reported values for Ta_3N_5 film,[10,24] nanorod[7,17] and nanoporous[18] photoanodes modified with CoPi, IrO_x, FeOOH and NiOOH co-catalysts. For the CoPi/GaN/Ta_3N_5 photoanode, the onset potential was improved to 0.65 V_{RHE}. Mott–Schottky results evidenced that the depletion region in GaN/Ta_3N_5 started to be generated from 0.22 V_{RHE} which was much improved compared to that of 0.8 V_{RHE} for Ta_3N_5 (Figure S7), suggesting passivation of the Ta_3N_5 surface states by the GaN (Figure S8). However, the valence band offset between GaN and Ta_3N_5 requires an additional external overpotential to transport holes from the Ta_3N_5 to the GaN for water oxidation, resulting in the onset potential of 0.65 V_{RHE}. We experimentally affirmed this improved PEC onset potential by fabricating GaN/Ta_3N_5 using a different process to evaporate metallic Ga onto the Ta_3N_5 followed by nitriding the Ga/Ta_3N_5 under the same conditions. Thus, GaN overcoating is a valid strategy and future improvement can be expected by forming a buried p/n junction of p-type GaN on n-type Ta_3N_5.

Beyond the onset potentials, a sharp rise in the photocurrent density was obtained. The photocurrent density of the CoPi/GaN/Ta_3N_5 photoanode was over 8 $mA cm^{-2}$ at 1.2 V_{RHE} under simulated AM 1.5G illumination. No pronounced hysteresis was observed during forward and backward LSV scans for either of the photoanodes, suggesting efficient charge transfer and collection within photoanodes. As shown in Figure 2b, the hypothetical half-cell solar-to-hydrogen energy conversion efficiency (HC-STH, η) values calculated for PEC schemes, using the equation $\eta = (1.23 - V_{RHE})\, j\, 100\,\%$, reached 1.5 and 1.0% for the CoPi/GaN/Ta_3N_5 and CoPi/Ta_3N_5, respectively. Our best CoPi/GaN/Ta_3N_5 film photoanode was able to generate an 8.5 $mA cm^{-2}$ photocurrent density at 1.2 V_{RHE}. This elevated photocurrent density can potentially enable a solar energy conversion efficiency of greater than 10% in a standalone solar water splitting device with tandem photovoltaic cells in response to the absorbance of solar light above 600 nm.

Substantial differences were observed between the CoPi/Ta_3N_5 and CoPi/GaN/Ta_3N_5 photoanodes in terms of the photocurrent stability as estimated by chronoamperometry. As shown in Figure 2c, the CoPi/Ta_3N_5 photoanode exhibited a large photocurrent density of 7.5 $mA cm^{-2}$ at 1.2 V_{RHE} during the initial stage of the PEC measurements, but this value decreased drastically over time, to almost nil after 1 h. No obvious recovery of the PEC performance was obtained after re-loading CoPi onto the CoPi/Ta_3N_5 photoanode (Figure S9). In clear contrast, a stable photocurrent density of 8 $mA cm^{-2}$ was obtained over 10 h under the same PEC conditions for the CoPi/GaN/Ta_3N_5 (Figure 2c). Bubbles were continuously generated during these PEC *j*-*t* tests. As evidenced by the electro-impedance spectroscopy (EIS) analyses obtained under the same PEC conditions in Figures 2d and e, the interfacial resistance between the CoPi/Ta_3N_5 and the electrolyte was drastically increased, to 12 kΩ, during the 1.5 h PEC test. This is attributed to the formation of highly resistive TaO_x layers on the Ta_3N_5, as discussed in detail below based on TEM evidence. In comparison, the interfacial resistance for the CoPi/GaN/Ta_3N_5 was slightly increased, by about 80 Ω, during the 10 h *j*-*t* test.

STEM and EDS analyses were conducted to clarify photoactivity loss for a CoPi/Ta_3N_5 photoanode after a 1.5 h PEC test. As shown in the cross-sectional STEM and EDS mapping images in Figure S10, a surface oxide layer was clearly present on the Ta_3N_5 after the test. Because the O signal may have been partly due to the CoPi, an EDS line scan analysis in TEM was used to investigate another pristine Ta_3N_5 photoanode without surface modification of CoPi after a 1 h PEC stability test. Figure S11 shows a clear O signal from the Ta_3N_5 surface, with an estimated thickness of 50 nm. It suggests that self-oxidation of Ta_3N_5 to form highly resistive TaO_x is the chief mechanism degrading the PEC performance of Ta_3N_5 during solar water oxidation. In contrast, a clear CoPi/GaN/Ta_3N_5 structure was observed in the case of the CoPi/GaN/Ta_3N_5 photoanode after a 10 h PEC *j*-*t* test (Fig-

ure S12), suggesting that the GaN functioned as a shield layer to protect the Ta_3N_5 from photo-oxidation. A prolonged PEC stability test of > 50 h was further performed using the CoPi/GaN/Ta_3N_5. As shown in Figure S13, the photocurrent gradually degraded over the last 40 h under continuous illumination. Based on SEM and EDS observations, we determined that the GaN layer was stable on the Ta_3N_5 during the 50 h test but the electrolyte gradually penetrated through pinholes in the GaN/Ta_3N_5 structure to oxidize the bulk Ta_3N_5 (Figure S14). We anticipate that CoPi/GaN/Ta_3N_5 will show long-term stability if the GaN can be conformally deposited on Ta_3N_5 without pinholes.

To confirm that oxygen evolution reactions (OERs) and hydrogen evolution reactions (HERs) occurred at the CoPi/GaN/Ta_3N_5 photoanode and the Cr-coated Pt cathode, the evolved gases from both electrodes were quantified by gas chromatography (GC), while recording the charges passing through the outer PEC circuit in situ. The CoPi/GaN/Ta_3N_5 photoanode was held at a constant bias of 1.2 V_{RHE} in a three-electrode configuration under simulated AM 1.5G illumination, and the evolved amounts of O_2 and H_2 were measured at 20 minutes intervals by GC over 12 h. The quantities of O_2 and H_2 evolved from the CoPi/GaN/Ta_3N_5 photoanode and the Cr-coated Pt cathode were found to be 670 and 1354 μmol cm^{-2} over 12.7 h. No increase in the N_2 concentration was detected during the test, indicating that the system was air-tight and there was no severe self-oxidation of the CoPi/GaN/Ta_3N_5 photoanode to generate N_2. Stoichiometric H_2 and O_2 evolution at a molar ratio of almost 2 was obtained with Faraday efficiencies for the HER and OER both close to 100% under ambient conditions (Figure 3).

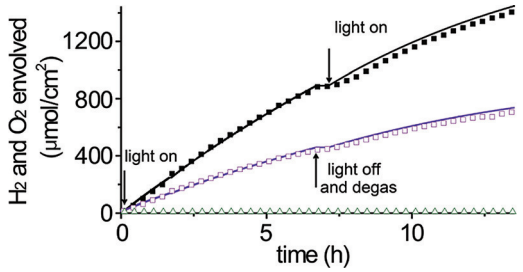

Figure 3. H_2 and O_2 evolution from the CoPi/GaN/Ta_3N_5 photoanode at 1.2 V_{RHE} under simulated AM 1.5G illumination. The amount of N_2 in the PEC cell during PEC tests was assessed. The solid lines represent H_2 and O_2 evolution at 100% Faraday efficiency calculated from the in situ charge measurements. Purple: O_2, black: H_2, green N_2. Area of the photoanode: 0.1 cm^2.

The effect of thickness and synthetic temperature for GaN coating on the PEC performance of the CoPi/GaN/Ta_3N_5 was assessed. As shown in Figure S15 and S16, coating of 50 nm GaN synthesized at 1273 K delivered the highest PEC performance and stability. Grazing incidence XRD analysis was conducted to better understand the depth-resolved crystalline properties concerning the bulk Ta_3N_5 in the GaN(ca. 50 nm)/Ta_3N_5 samples made at varying temperatures. It was evidenced in Figure S17 that an appreciable amount of the Ta_5N_6 phase was formed in the GaN/Ta_3N_5 at temperatures above 1373 K. This agrees with the phase transformation process[31] of TaN (873–1073 K)→Ta_3N_5 (1073–1273 K)→Ta_5N_6 (1073–1373 K)→ε-TaN (> 1573 K) during the nitridation of Ta in NH_3. The formation of Ta_5N_6 defects within the Ta_3N_5 is thus detrimental to the PEC performance[7,16] as it was also evident from Figure S16.

Scanning transmission electron microscopy (STEM) and energy dispersive spectroscopy (EDS) analyses were used to determine the structure and composition of the best performing GaN/Ta_3N_5 film. The cross-sectional STEM and corresponding EDS images in Figures 4 a–e and Figure S18 present

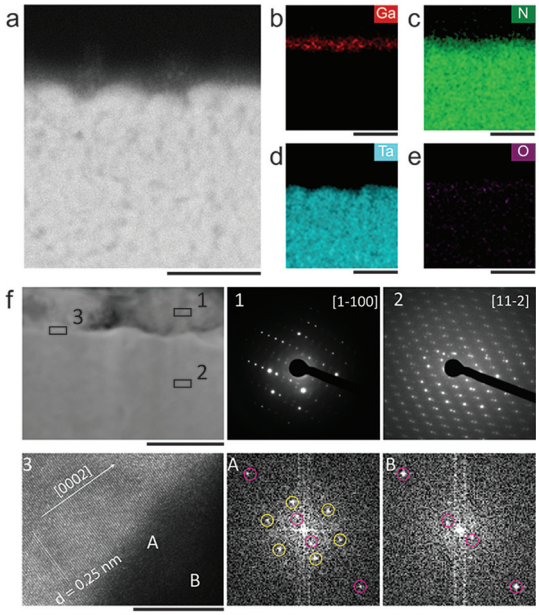

Figure 4. a–e) Cross-sectional EDS mapping images of a GaN/Ta_3N_5 STEM image. The scale bar is 100 nm. f) Cross-sectional STEM image of GaN/Ta_3N_5. The scale bar is 100 nm. Inset 1) is an ED pattern acquired from the GaN region, inset 2) is an ED pattern acquired from the Ta_3N_5 region and inset 3) is an HRTEM image with the corresponding FTED patterns acquired at region A of the GaN/Ta_3N_5 interface and region B of the Ta_3N_5. The scale bar is 10 nm.

the structure of a 50 nm thick GaN layer on a 500 nm Ta_3N_5 film. The EDS Ta signal is confined to the lower part while the EDS Ga signal is above the Ta_3N_5. Compared to the N signal, the O signal is minimal throughout the entire GaN/Ta_3N_5 sample. A thin Ta diffusion layer is observed at the GaN/Ta_3N_5 interface, as shown in the EDS line scan in Figure S19. This layer probably results from the high temperature nitridation at 1273 K.

To assess the crystal quality of the GaN and Ta_3N_5 and their interface, electron diffraction (ED) analyses were carried out. ED patterns acquired at region 1 of the upper GaN and region 2 of the lower Ta_3N_5 clearly show that the GaN and Ta_3N_5 were both crystalline (Figure 4 f). This result is in good agreement with the XRD data (Figure S6), and confirms that crystalline GaN/Ta_3N_5 was synthesized without forming other defective phases. As can be seen in the high-resolution TEM (HRTEM) image and the corresponding Fourier transform electron diffraction (FTED) patterns in

Figure 4 f, a distinct GaN/Ta_3N_5 interface was present. Lattice fringes with a spacing of 0.25 nm were generated by the GaN (Figure 4 f), which is consistent with the {002} plane spacing in wurtzite GaN. The FTED pattern at the interface demonstrates that the interface was composed of crystalline wurtzite GaN, as indicated by the yellow circles, and crystalline monoclinic Ta_3N_5, as indicated by the red circles. The quality of the GaN/Ta_3N_5 interface is considered to be crucial for efficient charge transfer and thus enabling high PEC performance.

In summary, CoPi/GaN/Ta_3N_5 film photoanodes were fabricated via newly developed sputtering–nitridation and evaporation–nitridation processes, to ensure stable and efficient solar water splitting. Photoanodes made from the resulting Ta_3N_5 films exhibited a high solar water splitting photocurrent density of 7.5 mA cm^{-2} at 1.2 V_{RHE}, owing to the successful synthesis of the vital TaO_δ precursor. The primary mechanism by which the performance of Ta_3N_5 is degraded is self-oxidation that forms highly resistive TaO_x at the Ta_3N_5 surfaces. After GaN coating to form a nitride-on-nitride structure with crystalline interfaces, a stable, high solar water splitting photocurrent density of 8 mA cm^{-2} was achieved at 1.2 V_{RHE} with H_2 and O_2 generated with unit Faraday efficiency over 12 h. Further enhanced solar water splitting durability with an improved onset potential can be expected with conformal overcoating of p-type GaN on n-type Ta_3N_5 films to form buried p/n junctions, with the eventual aim of obtaining low-cost, high-efficiency devices for solar fuel generation. The simple sputtering and evaporation steps described herein are readily applicable to the fabrication of a number of promising (oxy)nitrides that absorb at long wavelengths for practical PEC systems.

Acknowledgements

This work was financially supported by the Artificial Photosynthesis Project of the New Energy and Industrial Technology Development Organization (NEDO). A part of this work was conducted at Advanced Characterization Nanotechnology Platform of the University of Tokyo, supported by "Nanotechnology Platform" of the Ministry of Education, Culture, Sports, Science and Technology (MEXT), Japan.

Conflict of interest

The authors declare no conflict of interest.

Keywords: electrochemistry · photoanodes · photochemistry · solar energy conversion · water splitting

How to cite: *Angew. Chem. Int. Ed.* **2017**, *56*, 4739–4743
Angew. Chem. **2017**, *129*, 4817–4821

[1] M. Grätzel, *Nature* **2001**, *414*, 338–344.
[2] S. Hu, M. R. Shaner, J. A. Beardslee, M. Lichterman, B. S. Brunschwig, N. S. Lewis, *Science* **2014**, *344*, 1005–1009.
[3] M. Zhong, T. Hisatomi, et al., *J. Am. Chem. Soc.* **2015**, *137*, 5053–5060.
[4] M. G. Kibria, F. A. Chowdhury, S. Zhao, B. AlOtaibi, M. L. Trudeau, H. Guo, Z. Mi, *Nat. Commun.* **2014**, *6*, 6797.
[5] Q. Wang, T. Hisatomi, et al., *Nat. Mater.* **2016**, *15*, 611–615.
[6] M. Zhong, Y. Li, Y. Yamada, J.-J. Delaunay, *Nanoscale* **2012**, *4*, 1509–1514.
[7] Y. Li, T. Takata, D. Cha, K. Takanabe, T. Minegishi, J. Kubota, K. Domen, *Adv. Mater.* **2013**, *25*, 125–131.
[8] J. H. Kim, Y. Jo, J. H. Kim, J. W. Jang, H. J. Kang, Y. H. Lee, D. S. Kim, Y. Jun, J. S. Lee, *ACS Nano* **2015**, *9*, 11820–11829.
[9] M. Higashi, K. Domen, R. Abe, *J. Am. Chem. Soc.* **2012**, *134*, 6968–6971.
[10] C. Zhen, H. Cheng, et al., *Chem. Commun.* **2013**, *49*, 3019–3021.
[11] C. Leroy, A. E. Maegli, K. Sivula, T. Hisatomi, N. Xanthopoulos, E. H. Otal, S. Yoon, A. Weidenkaff, R. Sanjinesd, M. Grätzel, *Chem. Commun.* **2012**, *48*, 820–822.
[12] C. Wang, T. Hisatomi, et al., *J. Phys. Chem. C* **2016**, *137*, 15758–15764.
[13] K. Maeda, M. Higashi, B. Siritanaratkul, R. Abe, K. Domen, *J. Am. Chem. Soc.* **2011**, *133*, 12334–12337.
[14] M. Matsukawa, M. Ishikawa, et al., *Nano Lett.* **2014**, *14*, 1038–1041.
[15] S. Chen, S. Shen, G. Liu, Y. Qi, F. Zhang, C. Li, *Angew. Chem. Int. Ed.* **2015**, *54*, 3047–3051; *Angew. Chem.* **2015**, *127*, 3090–3094.
[16] C. Wang, T. Hisatomi, et al., *Chem. Sci.* **2016**, *7*, 5821–5826.
[17] L. Wang, F. Dionigi, N. T. Nguyen, R. Kirchgeorg, M. Gliech, S. Grigorescu, P. Strasser, P. Schmuki, *Chem. Mater.* **2015**, *27*, 2360–2366.
[18] G. Liu, S. Ye, P. Yan, F. Xiong, P. Fu, Z. Wang, Z. Chen, J. Shi, C. Li, *Energy Environ. Sci.* **2016**, *4*, 5028–5034.
[19] M. W. Kanan, D. G. Nocera, *Science* **2008**, *321*, 1072–1075.
[20] B. AlOtaibi, M. Harati, Z. Mi, et al., *Nanotechnology* **2013**, *24*, 175401.
[21] M. Zhong, Y. Ma, P. Oleynikov, K. Domen, J.-J. Delaunay, *Energy Environ. Sci.* **2014**, *7*, 1693–1699.
[22] T. Hayashi, M. Deura, K. Ohkawa, *Jpn. J. Appl. Phys.* **2012**, *51*, 112601.
[23] W. Chun, A. Ishikawa, H. Fujisawa, et al., *J. Phys. Chem. B* **2003**, *107*, 1798–1803.
[24] V. Stevanović, S. Lany, D. S. Ginley, et al., *Phys. Chem. Chem. Phys.* **2014**, *16*, 3706–3714.
[25] Z. Z. Bandić, P. M. Bridger, E. C. Piquette, T. C. McGill, *Appl. Phys. Lett.* **1998**, *72*, 3166–3168.
[26] J. Mickevičius, M. S. Shur, R. S. Q. Fareed, J. P. Zhang, R. Gaska, G. Tamulaitis, *Appl. Phys. Lett.* **2005**, *87*, 241918.
[27] S. Hafiz, S. Metzner, F. Zhang, M. Monavarian, V. Avrutin, H. Morkoç, C. Karbaum, F. Bertram, J. Christen, B. Gil, Ü. Özgür, *Proc. SPIE-Int. Soc. Opt. Eng.* **2014**, *8986*, 89862C.
[28] K. Kumakura, T. Makimoto, N. Kobayashi, T. Hashizume, T. Fukui, H. Hasegawa, *Appl. Phys. Lett.* **2005**, *86*, 052105.
[29] M. de Respinis, M. Fravventura, F. F. Abdi, H. Schreuders, T. J. Savenije, W. A. Smith, B. Dam, R. van de Krol, *Chem. Mater.* **2015**, *27*, 7091–7099.
[30] A. Ziani, E. Nurlaela, D. S. Dhawale, D. A. Silva, E. Alarousu, O. F. Mohammed, K. Takanabe, *Phys. Chem. Chem. Phys.* **2015**, *17*, 2670–2677.
[31] N. Terao, *Jpn. J. Appl. Phys.* **1971**, *10*, 248–259.

Manuscript received: January 5, 2017
Revised: February 15, 2017
Final Article published: March 21, 2017

